SANDIA REPORT

Active Assembly for Large-Scale Manufacturing of Integrated Nanostructures

Erik D. Spoerke, George D. Bachand, Judy K. Hendricks, Christopher Orendorff, Carolyn Matzke, Bonnie B. McKenzie, Bruce C. Bunker

Sandia National Laboratories

Active Assembly for Large-Scale Manufacturing of Integrated Nanostructures

Erik D. Spoerke, Chris Orendorff, and Bruce C. Bunker
Electronic and Nanostructured Materials Department
Sandia National Laboratories
P.O. Box 5800
Albuquerque, New Mexico 87185-MS1411

George D. Bachand, Judy K. Hendricks, and Carolyn Matzke
Biomolecular Interfaces and Systems Department
Sandia National Laboratories
P.O. Box 5800
Albuquerque, New Mexico 87185-MS1413

ABSTRACT

Microtubules and motor proteins are protein-based biological agents that work cooperatively to facilitate the organization and transport of nanomaterials within living organisms. This report describes the application of these biological agents as tools in a novel, interdisciplinary scheme for assembling integrated nanostructures. Specifically, selective chemistries were used to direct the favorable adsorption of active motor proteins onto lithographically-defined gold electrodes. Taking advantage of the specific affinity these motor proteins have for microtubules, the motor proteins were used to capture polymerized microtubules out of suspension to form dense patterns of microtubules and microtubule bridges between gold electrodes. These microtubules were then used as biofunctionalized templates to direct the organization of functionalized nanocargo including single-walled carbon nanotubes and gold nanoparticles. This biologically-mediated scheme for nanomaterials assembly has shown excellent promise as a foundation for developing new biohybrid approaches to nanoscale manufacturing.

ACKNOWLEDGMENTS

CONTENTS

FIGURES

NOMENCLATURE

mg	milligram
mL	milliliter
μL	microliter
μm	micrometer
MT	microtubule
DOE	Department of Energy
SNL	Sandia National Laboratories

1.0 INTRODUCTION

The explosion of interest in nanomaterials research in recent years has highlighted nanomaterials assembly as one of the primary challenges impeding the widespread application of nanotechnology. Certainly, the synthesis of technologically interesting nanomaterials has developed faster than the methods needed to integrate and organize these materials into functional device structures. Nanoscale assembly has been attempted using a variety of techniques such as Langmuir-Blodgett assembly,[1] microfluidic assembly,[2] electrical methods,[3] and nanomanipulation.[4] These assembly methods, however, either provide scalability *or* precise control, but generally not both. Ideally, nanoscale assembly methods will allow for precise manipulation of the nanostructures on a very local scale, while remaining applicable for large scale processing.

Biology continues to reveal itself as an exciting source of inspiration in the development of a system to address these assembly design requirements. In many living systems biomolecular agents, such as microtubules and motor proteins, act cooperatively to direct the precise organization of intracellular materials into complex, functional biological architectures. For example, in diatomaceous algae, kinesin motor proteins are believed to transport silica particles along microtubule networks to create the exquisitely complex protective "shells" of the diatoms. In the more dynamic example of some color changing fish, kinesin motors are responsible for the trafficking of pigment vesicles along microtubule networks to facilitate color change. These successful biological organizational and assembly processes rely on several key characteristics not generally utilized in typical synthetic materials assembly strategies. One such characteristic is that microtubules and motor proteins have very specific, selective interactions with one-another which facilitates great control over the assembly process. In addition, the assembly processes themselves are driven by the conversion of soluble chemical energy in the form of adenosine triphosphate (ATP) which additionally allows the process to be activated on a relatively large scale. These traits make microtubules and motor proteins attractive as tools for assembly of technological materials.

Microtubules and motor proteins have already stimulated significant interest as technological tools involved in nanocargo transport and sensing.[5-11] These applications frequently take advantage of an "inverted motility assay," where motor proteins are used to transport microtubules over a surface.[5, 12] In this assay, casein proteins are first adsorbed onto a substrate surface such as silica (glass) or gold. This protein layer, then, serves to organize the subsequent attachment of motor proteins (such as *Drosophila* kinesin) to the substrate surface in such a way that the moving "heads" of the motor proteins are displayed off the surface. Microtubules introduced to these ATP-driven motors will then be captured and transported over the surface in an arrangement that is inverted with respect to normal motility in a cell where the motors commonly move over microtubule arrays.

This report will describe an adaptation of this assay whereby motor proteins and microtubules are used as tools in a scalable approach to assembly of integrated nanostructures. In particular it focuses on the development of a novel methodology which combines surface-selective chemical treatments with bioselective interactions between microtubules and motor proteins to create patterned microtubule networks. By further using specific biochemical functional groups, we show that it is possible to use these engineered microtubule networks as templates to organize other nanomaterials such as carbon nanotubes and gold nanoparticles.

2.0 METHODS AND MATERIALS

All tubulin was obtained from Cytoskeleton, Inc (Denver, CO). Chemical reagents were provided by Sigma (St. Louis, MO).   Fluorescent streptavidin was obtained from Invitrogen, Inc. (Carlsbad, CA).

2.1. Selective Functionalization of Gold/Silica Micropatterns

Micropatterns of gold on silica surfaces (silica coating over single crystal silicon) were created by standard lithographic techniques commonly used at Sandia. These substrates were then diced into small samples (~3mm x 9mm), each piece containing two different micropatterned structures. These structures are visible in Figure 1 below.
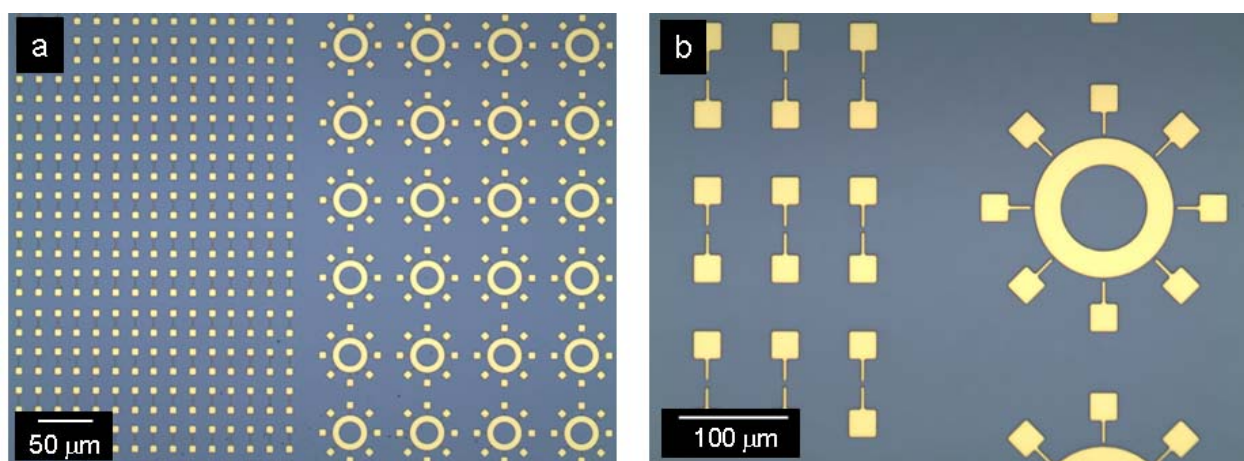
Figure 1. A photomicrograph of lithographically patterned gold electrodes on an oxidized silicon substrate. Test pads are each 25 μm on each side, gold lines are 3   μm wide and the gold rings are 25 μm thick. Test gaps between structures are 3-5 μm wide.

Substrates were cleaned for 15 minutes in acetone, dried, and treated for 20 minutes in an oxidizing solution containing a 1:1 ratio of concentrated sulfuric acid (H_2SO_4) and 30% hydrogen peroxide (H_2O_2). After rinsing in deionized water and air-drying, the substrates were then incubated for 20 minutes in a 10 mM solution of 3-aminopropyltriethoxysilane (APTES) in acetone. Substrates were then rinsed in acetone, air-dried and annealed for 20 minutes at 60°C in air.

2.2. Biofunctionalization and Microtubule Network Formation

Substrate treatments at this stage were modified from simple immersion-based incubations to surface-restricted incubations illustrated schematically in figure 2. Samples were inverted onto a bubble of incubation solution contained in a plastic concave sample container (a wafer shipper). Not only does this approach minimize the quantity of reagent needed to perform each incubation, but it insures that only the sample surface of interest will be in contact with any

8

incubating or reacting solution. Furthermore, since the sample surface is always located above the solution, this methodology minimizes non-specific binding of aggregates which may settle through the incubation solution.
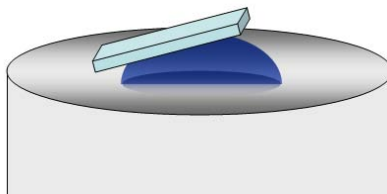
Figure 2. Illustration of the "surface-selective" incubation scheme. Substrates are inverted over a small droplet of incubation solution, allowing only the desired surface to contact the solution and preventing undesired aggregate settling on the substrate surface.

Applying this "inverted bubble" approach, the amine-functionalized substrates were first incubated for 10 minutes over 100 microliters of 0.5 mg/mL casein in aqueous BRB80 (80 mM piperazinebis(ethanesulfonic acid), 1 mM $MgCl_2$, 1 mM ethylene glycol bis(b-aminoethyl ether-N,N,N,',N'-tetraacetic acid (EGTA), pH 6.9). After 10 minutes, 50 µL of this solution was replaced with 39.5 µL of BRB80 0.5 µL 100mM magnesium adenosinetriphosphate (MgATP), and 10 µL of 6 µg/mL purified *Drosophila* kinesin.

Meanwhile, fluorescein-labeled tubulin, diluted 1:1 with unlabeled tubulin, was polymerized at a concentration of 5mg/mL in BRB80P ((BRB80 + 10% glycerol + 1 mM GTP) by incubation at $37^{o}C$ for 20-30 minutes. The polymerized microtubules were stabilized by the addition of 100 µL of BRB80T (BRB80 + 10 mM paclitaxel) and stored at room temperature for later use.

After incubation with kinesin, excess liquid was wicked away from the substrates and they were quickly placed over a fresh solution containing 25 µL of polymerized microtubules in BRB80T plus 0.5 µL of either 100mM MgATP or the non-hydrolyzable analog to ATP, adenyl-5'-yl imidodiphosphate (AMPPNP). The substrates were allowed to incubate thus for approximately 30 minutes to allow microtubules to attach to the substrate surface.

2.3. Loading Microtubule Networks with Nanocargo

The principal nanocargo used to demonstrate attachment to microtubules were single wall carbon nanotubes (SWNTs). These carbon-based nanotubes are an attractive choice because they exhibit a variety of potentially useful characteristics such as electrical conductivity, semiconductivity, and photothermal behavior. A secondary type of nanocargo explored was gold nanoparticles, which have also been shown to demonstrate technologically useful properties such as electrical conductivity and photothermal behavior.

The SWNTs were provided by Elena Bekyarova of Professor Robert Haddon's laboratory at the University of California at Riverside. These SWNTs were acid-modified and subsequently covalently functionalized with fluorescently-labeled streptavidin. Excess streptavidin was removed by combined centrifugation and dialysis. Immediately prior to use, these SWNTs were

sonicated for 5 minutes and diluted (commonly by a factor of 2) in BRB80T containing 1 mM AMPPNP.

The synthesis of spherical gold nanoparticles (diameter = 18 nm) was adapted from the boiling citrate reduction method described by Frens.[13] Specifically, 100 mL of aqueous 2.5×10^{-4} M $HAuCl_4$ was heated to boiling. Once boiling, 10 mL of aqueous 1% sodium citrate was added and continued to boil for > 1 h. The solution underwent color changes from purple to ruby red, indicating the formation of the desired particles. The nanoparticle solution was cooled to ambient temperature and stored in the dark to minimize photooxidation. Nanoparticles were then biotinylated using a similar procedure described by Caswell et al.[14] A 3.7×10^{-3} M stock solution of N-(6-(Biotinamido)hexyl)-3'-(2'-pyridyldithio)-propionamide (biotin-HPDP) was prepared in DMF. To 1 mL purified nanorods, add 10 μL of 3.7×10^{-4} M biotin-HPDP in H_2O. After 4 h, modified nanorods were centrifuged at 5,000 RPM for 5 min and redispersed in 1 mL deionized water. Prior to use, these biotinylated particles were treated with 1:100 diluted fluorescent streptavidin (Oregon Green 488) for 10 minutes. Particles were then centrifuged at 14,000 rpm for 10 minutes to remove excess streptavidin. These particles were then resuspended in BRB80T containing 1 mM AMPPNP by brief sonication and agitated pipeting

In both the SWNT and gold nanoparticle cases, 50-100 μL droplets of dispersed suspensions were placed in an incubation container (as above) and the MT-decorated substrates (wicked, but still wet) were immediately placed face-down on top of the droplets for a 20 minute incubation. Samples were then removed from solution and rinsed by placing the samples on three successive drops of clean BRB80T. The sample was finally placed face-down on a 15 μL droplet of BRB80TAF (BRB80T + 20mM dextrose + 0.02mg/mL glucose oxidase, 8 μg/mL catalase, and 0.5% β-mercaptoethanol) on a glass coverslip and fluorescence microscopy was used to image the assembled structures using an Olympus IX71 microscope with a 100X oil immersion lens and a Hamamatsu Orca II-ER CCD camera.

Electrical conductivity measurements were made on samples following examination under the fluorescence microscope. Samples were removed from the imaging coverslip and placed in a 1% glutaraldehyde in BRB80T for 30 minutes at room temperature. Samples were then dip-rinsed in deionized water or ethanol. Samples were then air dried and placed on a microscope stage fitted with microprobe positioners. Electrical resistance measurements were made using 3 μm diameter tungsten probe tips placed in contact with the lithographic gold structures.

3.0 RESULTS AND DISCUSSION

The results presented below illustrate how the selective functionalization of lithographic substrates was utilized to promote specific microtubule capture. Furthermore, the captured microtubules were then shown to serve as scaffolds onto which nanoscale cargo was loaded. The fluorescence micrographs in figure 3 reveal a number of significant results about the capture of microtubule networks.
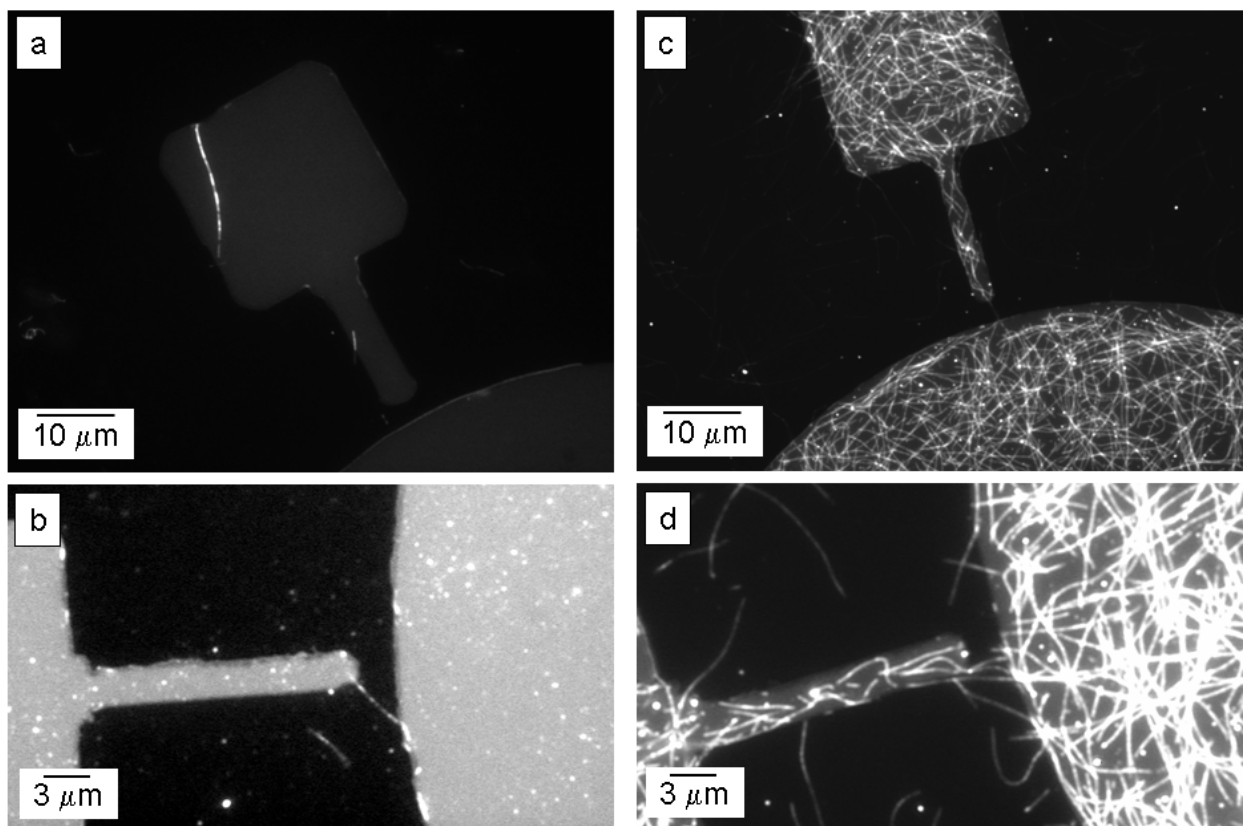
Figure 3. Fluorescence micrograph of selective MT capture by kinesin motor proteins in the presence of (a, b) ATP and (c, d) AMPPNP. (a and c) show selectivity of microtubules for the kinesin-coated gold pads, while (b and d) illustrate MT bridge formation. Capture using AMPPNP is notable more effective.

The first point of importance in figure 3 is the difference in MT capture by kinesins when AMPPNP is used instead of ATP. Figures 3a and 3b illustrate the motor-protein mediated capture of microtubules in the presence of ATP. In figure 3a, there are several microtubules visible, attaching very selectively to the outline of the gold micropatterns. Figure 3b even shows a microtubule forming a bridge between two gold structures. By comparison, however, figures 3c and 3d show microtubule capture using exactly the same preparation of the substrates and microtubules, but the ATP used to fuel the motors in 3a and 3b was replaced with the non-hydrolyzable analog to ATP, AMPPNP. As evident in figures 3c and 3d, the effectiveness of the capture is dramatically enhanced when AMPPNP is used. While figure 3c demonstrates the high density of MTs selectively bound to the gold pattern, figure 3d shows the formation of a microtubule bridge composed of not one, but several microtubules.

The second point to note about the images of figure 3 is the selectivity of the MT capture. This result speaks to the effectiveness of the specific functionalization of the silica surfaces with the aminosilane, decorating the silica with positively-charged amines, but leaving the gold surfaces unreacted. It has been previously shown that cationic, hydrophilic surfaces (such as the free amine-coated silica surface presented in our case) discourage the organization of casein, and

thus kinesin motors, in a way that promotes microtubule transport.[6] It is believed that the free amines displayed on our APTES-coated silica surfaces modify the adsorption of casein. These rearranged casein proteins consequently fail to properly arrange subsequent kinesin attachment to the silica surfaces in a way that allow the kinesin to effectively capture microtubules. Meanwhile, the gold surfaces, which are not reactive with the APTES, do promote proper casein and motor protein adsorption, followed by extensive, selective microtubule capture on the gold electrodes. Although there is a small degree of non-selective MT binding to the inter-electrode spaces, the selectivity of this approach is particularly impressive, considering that there are no particular protein-blocking agents (i.e. polyethylene glycol, etc) applied to those areas. In fact it is somewhat surprising that negatively charged surface groups are not more attracted to the positive charges of these free amines. This result speaks to the effective adsorption of casein as a blocking layer over the silica surfaces. Further investigation of surface treatments that combine surface amines with a designed protein blocking layer may prove more effective in reducing non-specific MT adsorption on the inter-electrode surfaces.

The attachment of technologically relevant materials to these bridged networks was demonstrated using single walled carbon nanotubes (SWNTs) and gold nanoparticles. Figure 4 displays fluorescent images illustrating the selective attachment of SWNTs to captured microtubules.
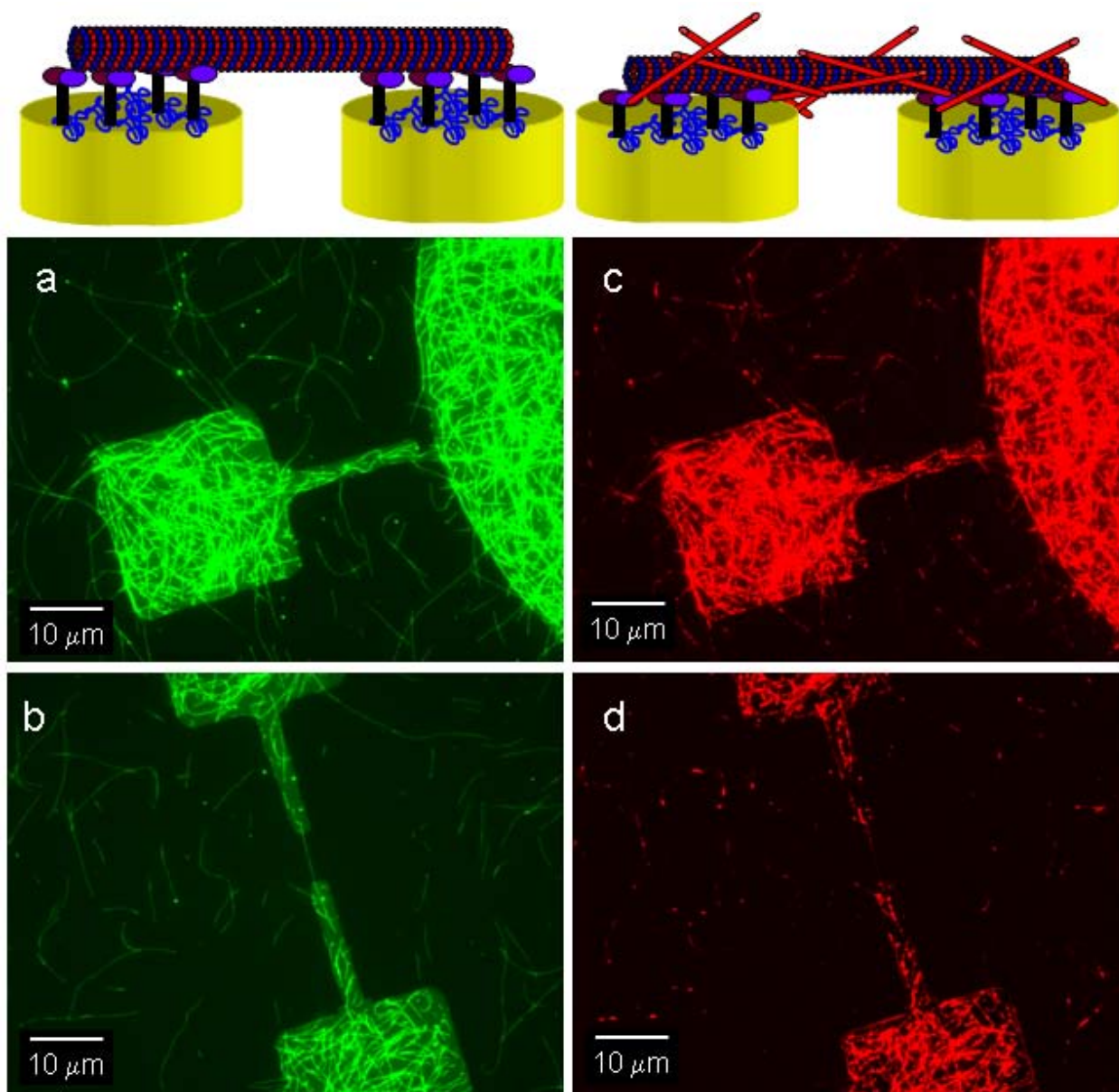
Figure 4. (a and b) Fluorescence micrographs (Ex: ~475nm) of microtubules selectively captured on gold pads. MT bridges are visible connecting gold structures. (c and d) Fluorescence micrographs (Ex: ~530nm) of SWNTs decorating the MTs from (a and b). Strong correlation of fluorescence indicates selective templating of the SWNTs onto the captured MTs. Careful examination even shows SWNTs spanning the test gaps along the MT bridges. *Green and red coloration added artificially to grayscale images to reflect what was seen by eye.

In figures 4a and 4b, green fluorescent microtubules (Ex: ~ 475nm) are shown densely coating patterned gold electrodes and forming bridges between closely-spaced gold structures. Figures 4c and 4d show these same microtubule networks under different fluorescent excitation (Ex: ~ 530nm), which elicits emission only from the fluorescent streptavidin conjugated to the SWNTs. The resulting red fluorescence visible in the image identifies single walled carbon

nanotubes (SWNTs) bound to the microtubules. Control experiments where the SWNT suspension was filtered through a 0.2 mm filter (large enough to allow free streptavidin to pass through the filter) produced no fluorescence at 530nm excitation. This control confirms that the red fluorescence is in fact emitted from SWNTs bound to the MTs, and the detected fluorescence is not a false positive generated by free molecular streptavidin.

There is a very clear correlation between the red fluorescence of the SWNTs and the green fluorescence of the MTs. This strong correlation clearly illustrates the selective binding of the SWNTs to the MT scaffolding. In fact, the SWNTs are even visible spanning the MT bridges. Figure 5 is a high magnification scanning electron micrograph showing SWNT attachment to a microtubule. The microtubule, seen as the broad white swath of contrast (roughly 25-35 nm across) extending from the lower left to the upper right portion of the figures 5a and 5b. The carbon nanotubes are visible as meandering linear features approximately 1-2 nm wide decorating the MT surface. Three of the most clearly visible SWNTs (though there are more in the image) are illustrated by the colored arrows in figure 5a and both colored arrows and colored traces in figure 5b. This figure provides a very detailed picture of how the SWNTs attached to the MTs. They do not align as rigid structures, but appear to bend into winding forms as they attach to the MTs. In addition, it is clear that although the fluorescence images in figure 4 show correlation between the SWNTs and the MTs, the SWNT alignment is not perfectly registered with the long axis of the MTs. This mixed orientation may play an important role in establishing internanotube connections that would be critical for establishing electrical conductivity along the length of the MT template.
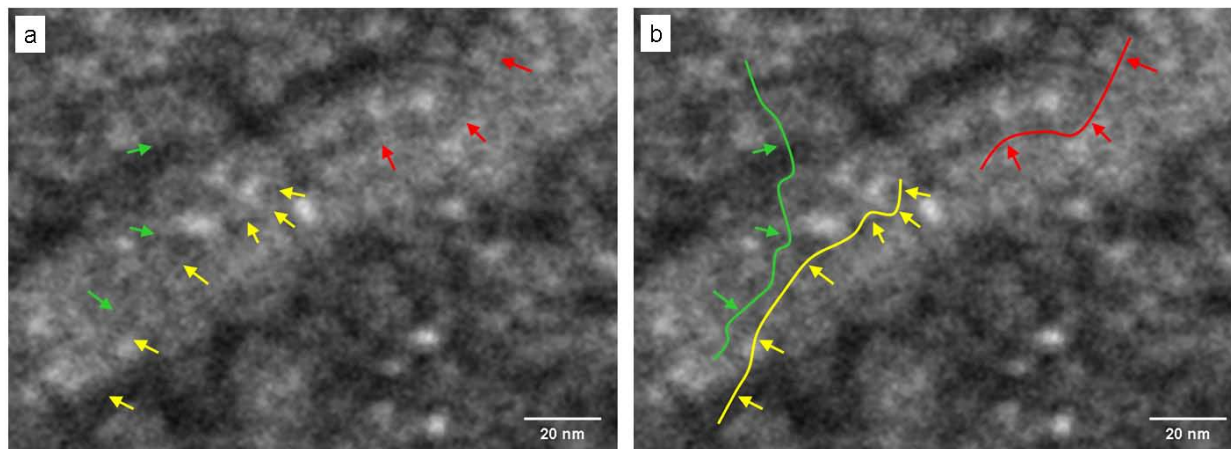

Figure 5. (a) A scanning electron micrograph of SWNTs (arrows) decorating a single MT. The MT is visible (slightly broadened due to drying for SEM) as the broad light swath extending from lower left to upper right. SWNTs are visible as winding linear structures attached to the MT. These SWNT are "traced" in (b) for clarity.
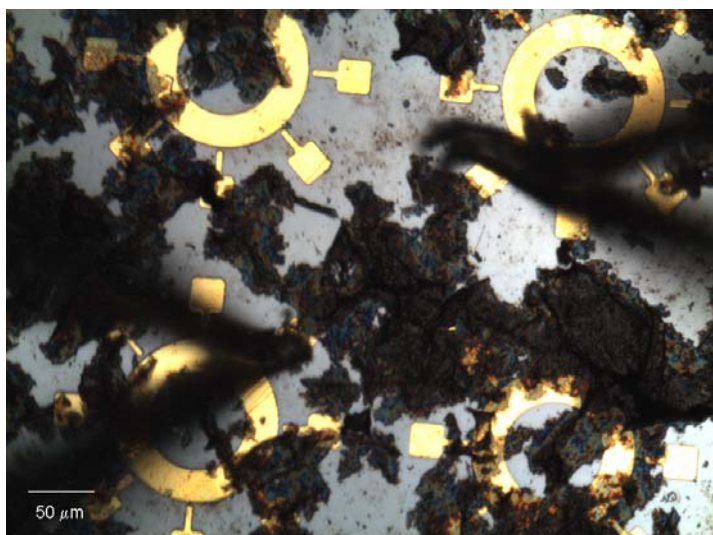
Figure 6. Photomicrograph of a dense mat of SWNTs non-specifically dried across separated gold patterns. Electrodes visible entering from above the substrate are contacting separated gold pads and are measuring approximately 30 kOhms across the SWNT mat.

Electrical conductivity was measured on these substrates, but no detectable current was found between MT/SWNT-bridged electrodes. By contrast, when positive controls were run where highly dense networks of SWNTs were non-selectively deposited over the electrodes, electrical connectivity between electrodes was detected, yielding a resistance of roughly 30 kOhms. An optical micrograph of these structures is shown in figure 6. This positive control indicates that electrical current can be passed through these SWNT connections, and further that the SWNTs are capable of sufficient connectivity to the gold electrodes to conduct electrons. These indications suggest that the lack of conductivity measured along the MT/SWNT bridges may be due to an overall lack of attachment density, and thus connectivity. Refinement of this attachment-based templating process in parallel, continuing research programs may help to increase nanocargo attachment density.

In addition to carbon nanotube attachment to the MT network templates, attachment of functionalized gold nanoparticles was also demonstrated. Two examples of these results are shown in figure 7.
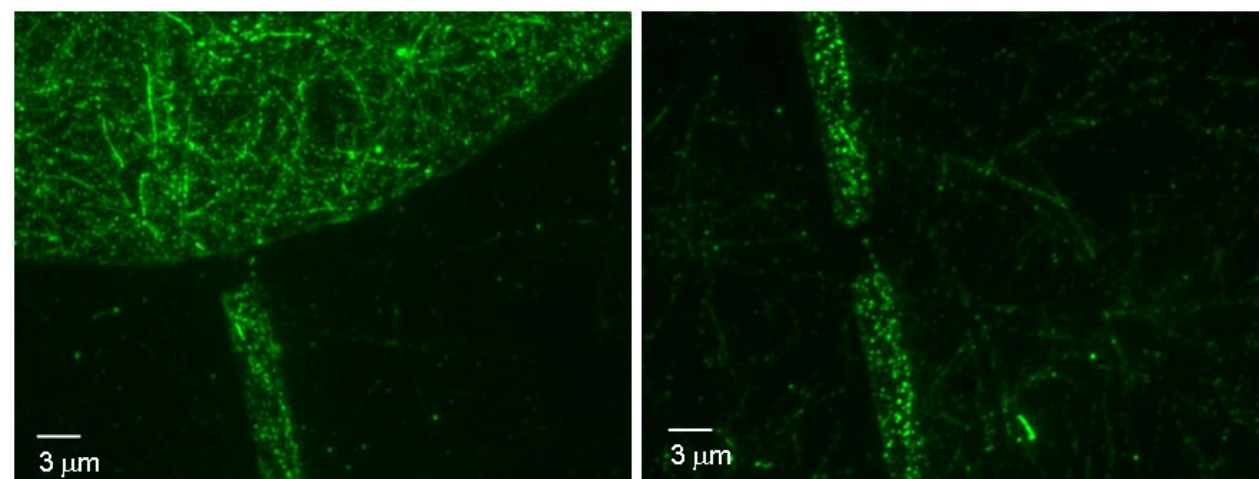

Figure 7. Fluorescent micrograph of fluorescently-tagged gold nanoparticles decorating captured MTs. In both images, the gold nanoparticles can be seen attached to MT bridges between gold structures.

The microtubules used in these cases contained no fluorescent labels, so the green fluorescence seen in these examples was exclusively emitted from the fluorescent streptavidin (Ex: 488) used to functionalize the biotinylated gold particles. There may have been a small degree of free streptavidin that bound to the biotinylated MTs, but the majority of the fluorescence seen in the images of figure 7 was the result of functionalized gold nanoparticles. The figure clearly shows a significant amount of gold binding to the captured MT networks, even decorating the MT bridges between the gold structures. The SEM images in figure 8 provide a closer look at the organization of the gold nanoparticles by the MT templates.
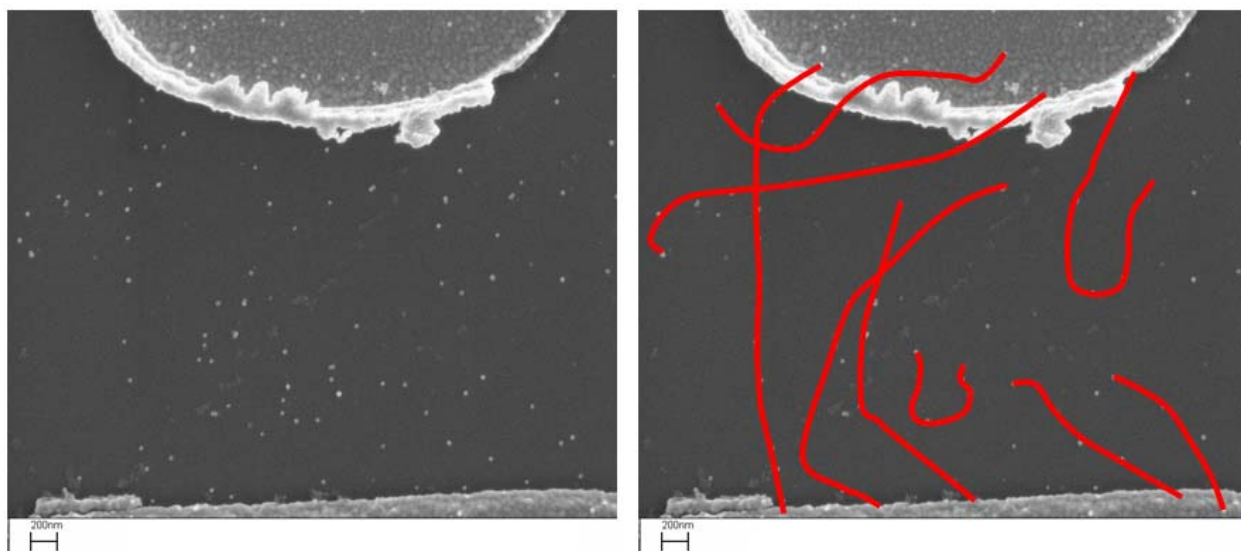
Figure 8. Scanning electron micrographs of gold nanocrystals templated across MT structures, including MT bridges between the gold test pads at the top and bottom of the image. The MTs are no longer visible in the image, but the gold particles have been clearly arranged in MT-templated patterns. The image on the right is an estimated trace of where the MTs were likely located when they templated the gold particles.

In figure 8a, the organic MT templates appear to have been largely destroyed, leaving behind only organized gold features. Figure 8b contains the same micrograph as in figure 8a, but the "missing" microtubules that templated the apparent gold nanoparticle patterns are drawn in. The disappearance of the MT networks is believed to be an artifact of the SEM characterization, whereby localized heating of the gold nanoparticles under the electron beam may have destroyed the organic microtubule templates. Figure 9 shows the correlation between the gold nanoparticle presence and the MT destruction clearly, where the MT in the image is only partially decorated with gold nanoparticles.

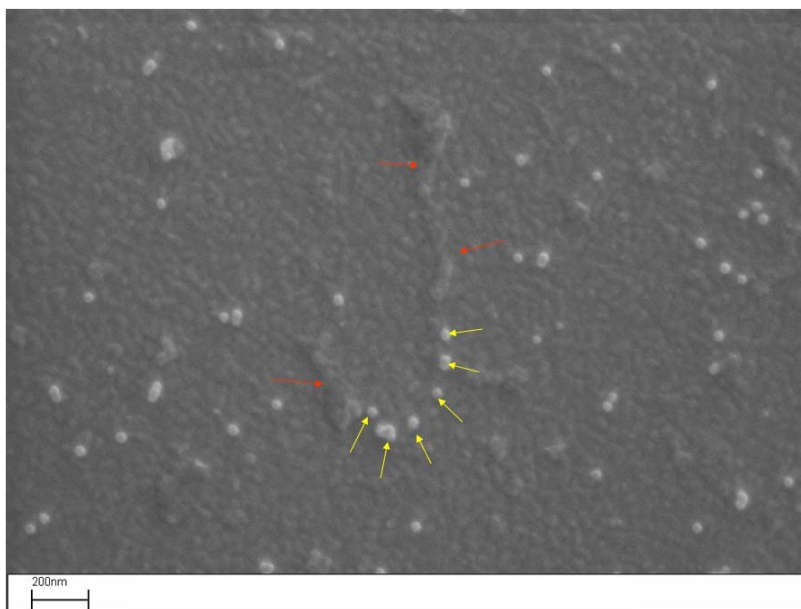**Figure 9.** A scanning electron micrograph of a "J-shaped" MT(red arrows), partially decorated with gold nanoparticles (yellow arrows). Where gold nanoparticles are bound to the MT, the MT appears to have been destroyed under the electron beam.

In the region where the gold nanoparticles are bound, the MT has been destroyed, but the MT remains largely intact where it is undecorated. This artifact is of significant interest because it presents a possible method to selectively remove the organic MT template without need to heat the entire sample, a treatment which may have adverse affects on device performance. Using electrical or optical means to elicit heat from the gold nanoparticles may allow for much more specific template removal.

Electrical conductivity measurements of these samples also failed to produce any measurable current. Based on the SEM images it would appear that this problem is also due to low nanoparticle loading on the MTs, resulting in inadequate interparticle connections along the MT template. Once again, future efforts on parallel research programs may help to either increase nanoparticle loading density or may lead to the use of other gold nanoparticle morphologies, such as nanorods or nanowires, which would both increase the likelihood of nanoparticle connection (possibly through entanglement of attached particles) and decrease the need for contacts due to the increase electrical persistence length of the rods.

4.0 CONCLUSIONS

This report describes a new approach to nanoscale materials assembly that utilizes the active, bioselective interactions of microtubules and kinesin motor proteins. Utilizing silica-selective amino-silane chemistry, proper casein-mediated kinesin adsorption was restricted to lithographic gold patterns on silica substrates. These selectively-bound kinesin motors were then shown to capture microtubules out of suspension to create networks. The specificity of the motors for the microtubules insured that microtubules were almost exclusively captured by kinesins bound to the gold structures, often bridging gaps between adjacent structures. These

organized microtubules were then demonstrated to be selective templates for attachment of technologically-relevant nanoscale cargo, specifically carbon nanotubes and gold nanoparticles. Utilizing bioselective biotin-streptavidin linkages, the nanocargo were shown to bind to the microtubule templates but nanocargo density was apparently insufficient to allow electrical conductivity through the templated nanomaterials. Overall, the materials and methods presented in this report as parts of a new strategy that uses the unique chemically and biologically selective characteristics of microtubules and motor proteins to direct nanoscale materials assembly.

5.0 REFERENCES

1. Kim, F.; Kwan, S.; Akana, J.; Yang, P., Langmuir-Blodgett Nanorod Assembly. *J. Am. Chem. Soc.* **2001,** 123, (18), 4360-4361.
2. Huang, Y.; Duan, X.; Wei, W.; Lieber, C., Directed-assembly of one-dimensional nanostructures into functional networks. *Science* **2001,** 291, 630.
3. Duan, X.; Huang, Y.; Cui, Y.; Wang, J.; Lieber, C., Indium phosphide nanowires as building blocks for nanoscale electronic and optoelectronic devices. *Nature* **2001,** 409, (6816), 66-36.
4. Wilms, M.; Conrad, J.; Vasileve, K.; Kreiter, M.; Wegner, G., Manipulation and conductivity measurements of gold nanowires. *Appl. Surf. Sci.* **2004,** 238, 490-494.
5. Bachand, G. D.; Rivera, S. B.; Boal, A. K.; Gaudioso, J.; Liu, J.; Bunker, B. C., Assembly and transport of nanocrystal CdSe quantum dot nanocomposites using microtubules and kinesin motor proteins. *Nano Letters* **2004,** 4, (5), 817-821.
6. Boal, A.; Bauer, J.; Rivera, S.; Manley, R.; Manginell, R.; Bachand, G.; Bunker, B., Monolayer Engineered Microchannels for Motor Protein Transport. *Langmuir (submitted)* **2006**.
7. Bohm, K.; Beeg, J.; zu Horste, G.; Stracke, R.; Unger, E., Kinesin-driven sorting machine on large scale microtubule arrays. *IEEE Trans on Adv Pack* **2005,** 28, (4), 571-576.
8. Bohm, K. J.; Stracke, R.; Muhlig, P.; Unger, E., Motor protein-driven unidirectional transport of micrometer-sized cargoes across isopolar microtubule arrays. *Nanotechnology* **2001,** 12, (3), 238-244.
9. Hess, H.; Clemmens, J.; Qin, D.; Howard, J.; Vogel, V., Light-controlled molecular shuttles made from motor proteins carrying cargo on engineered surfaces. *Nano Lett* **2001,** 1, (5), 235-239.
10. Hess, H.; Howard, J.; Vogel, V., A piconewton forcemeter assembled from microtubules and kinesins. *Nano Lett* **2002,** 2, (10), 1113-1115.
11. Jia, L.; Moorjani, S.; Jackson, T.; Hancock, W., Microscale Transport and Sorting by Kinesin Molecular Motors. *Biomed. Microdev.* **2004,** 6, (1), 67-74.
12. Howard, J.; Hunt, A.; Baek, S., Assay of Microtubule Movement Driven by Single Kinesin Molecules. *Methods Cell Bio* **1993,** 39, 137-147.
13. Frens, G., Controlled nucleation for the regulation of the particle size in monodisperse gold suspensions. *Nature* **1973,** 241, 20.
14. Caswell, K.; Wilson, J.; Bunz, U.; Murphy, C., Preferential end-to-end assembly of gold nanorods by biotin-streptavidin connectors. *J. Am. Chem. Soc.* **2003,** 125, 13914-13915.

Distribution:

1	MS 0123	D. Chavez, LDRD Office	01011
1	MS 0885	J. E. Johannes	01810
1	MS 0886	B.B. McKenzie	01822
1	MS 0887	D.B Dimos	01800
1	MS 1411	J.A. Voigt	01816
1	MS 1411	E.D. Spoerke	01816
1	MS 1411	C. Orendorff	01816
1	MS 1411	B.C. Bunker	01816
1	MS 1413	G.D. Bachand	08331
1	MS 1413	J.K. Hendricks	08331
2	MS 9018	Central Technical Files	08944
2	MS 0899	Technical Library	04536